Aerotecnica Missili & Spazio (2024) 103:3–15
https://doi.org/10.1007/s42496-023-00187-0

ORIGINAL ARTICLE

Estimation of the Thermophysical Properties of C/C Plates with Ceramic Nanocoating at Different SiO_2 Filling for Aerospace Applications

A. V. Morzhukhina[1] · O. M. Alifanov[1] · S. A. Budnik[1] · A. V. Nenarokomov[1] · D. M. Titov[1] · A. Delfini[2] · R. Pastore[2] · F. Santoni[2] · M. Albano[3] · M. Marchetti[2]

Received: 15 May 2023 / Revised: 22 October 2023 / Accepted: 27 October 2023 / Published online: 27 November 2023

Abstract

In aerospace industrial and commercial scenario, the reusable launch vehicles (RLV) evolution works constantly toward the lowering of payload conveyance expenses. The thermal protection system (TPS) preserves the integrity of the space vehicle surfaces exposed to huge thermal shock during the re-entry phase: its advanced design and manufacturing, aimed at both reusing and withstanding harsh space environment, result in increasing the production and maintenance charges. The present study introduces a cost-saving concept of TPS component made of carbon/carbon (C/C) tiles coated by a commercial refractory varnish reinforced with ceramic nanoparticles. Using a reliable computing method, known as inverse method, the thermophysical properties such as heat capacity and thermal conductivity of the manufactured materials are assessed in a broad range of temperatures, with the input aid of an in-house developed experimental setup. The described technique is especially suited for approaching such kind of issues, thanks to the capability of taking into account several physical variables simultaneously, with the aim of gaining a robust knowledge of materials' thermal behavior for potential use in spacecraft TPS.

Keywords Carbon-carbon · Nano-coating · Thermal protection system · Inverse method · Re-entry spacecraft · Thermo-mechanical stress

List of Symbols

Latin Symbols

b	Length of heat flux sensor
$C(T)$	Volumetric heat capacity
$f_m(\tau)$	Temperature measurements
$\overline{g^s}$	Vector of gradient minimization method at current iteration
J	Least-square minimized functional
$\overline{J'}_p^{(s)}$	Gradient of the functional J at current iteration
N_p	Number of unknown parameters
$\overline{p}$	Vector of unknown parameters
$q_1(\tau)$	Heat flux at the heated boundary
$q_2(\tau)$	Heat flux at the inner boundary
$T(\tau, x)$	Temperature
$T_0(x)$	Initial temperature
x	Spatial variable
$x_1, x_2, \ldots, x_M$	Coordinates of thermocouples
$X_1, X_2, \ldots, X_L$	Coordinates of layer boundaries

Greek Symbols

β^s	Parameter of conjugate gradient method at current iteration
$\overline{\gamma^s}$	Step descent
$\Delta T(x,\tau)\,\theta(x,\tau)$	Increment of temperature
δ_f	Integral error of temperature measurements
$\lambda(T)$	Thermal conductivity
$\sigma_m(\tau)$	Measurement variance
τ	Time

✉ R. Pastore
roberto.pastore@uniroma1.it

[1] Department of Space System Engineering, Moscow Aviation Institute, 4 Volokolamskoe hgw., Moscow 125993, Russian Federation

[2] Department of Astronautic, Electric and Energetic Engineering, Sapienza University of Rome, via Eudossiana 18, 00184 Rome, Italy

[3] Agenzia Spaziale Italiana, via del Politecnico snc, 00133 Rome, Italy

τ_m	Final time
$\psi(x, \tau)$	Adjoint variable for temperature (Lagrange multiplier)

Subscripts

k	Number of unknown parameters
l	Number of layers
m	Number of thermocouples

1 Introduction

The development of re-entry spacecraft enforces the concept of reusable integrated systems suited for handling the hard operating conditions of re-entry and in-orbit flight. Spacecraft are subjected to severe thermomechanical loads, outgassing damaging, ultraviolet and atomic oxygen exposure, as well as further aging agents that can badly affect the structural integrity of the vehicle. Testing and qualification of materials exposed to these extreme conditions have provided data to enable the manufacturing of long-life reliable components used on Earth as well as in the world's most sophisticated satellite and spacecraft subsystems, as reported by NASA ISS Program Science Office [1]. About the thermal conditions-induced degradation, the critical mechanical defects that can grow have to be identified and recorded by specialized detection methods and their impact in space has to be treated statistically, as reminded in reference MRS Bulletin [2]. In this regard, NASA Technical Reports as well as reference handbooks of environmental degradation of materials underline the need to have ever more detailed knowledge of the near-Earth thermal environment parameters and of system's thermal response time, with particular regard to the task of the effects of mismatch in the coefficient of thermal expansion (CTE) arising in not homogeneous materials such as composites or coated materials [3, 4]. About thermal control surfaces, a widely used concept is the application of protective coatings, which are stable under sthe pace environment, having good adhesion and with similar thermal expansion coefficient of the substrate, even if the adopted solutions have to face to the synergic enhanced degradation due to thermal outgassing and UV and atomic oxygen exposure [5, 6].

Advanced design and manufacturing solutions are required to provide effective and low-cost thermal protection systems (TPS), which should be thin, lightweight and reusable. Carbon/carbon (C/C) ceramic composites are ideal candidates to be used in space vehicles TPS, thanks to a huge thermomechanical resistance, even at temperatures of 1000°. This advanced composite material is the most advanced form of carbon, consisting of a fiber based on carbon precursors embedded in a carbon matrix; a few tens of companies in the world deal with some form of C/C composites, the major market share being kept by the US industrial segment, followed by French and British companies, while other countries with more focus on industrial rather than aerospace and military applications are Germany and Japan [7]. The various precursors of fibers as well as the methods of processing C/C matrix materials have direct influence on the characteristics of the final product, as widely studied; in particular, the C/C physical properties are determined by both the fine and coarse microstructural features and by the nature of the interface between fibers and matrix [8, 9]. Further complications arise from the use of subtle treatments such as surface modification of the fibers and inclusion of oxidation protection; the number of possible combinations of parameters is almost limitless, classifying C/C as a family of materials whose properties may be tailored to suit a specific application [10]. Despite long studies performed all over the world on this material, there are still not standard methods for its production. In particular, one of the most critical issues is to obtain uniform structures with high thickness: to this aim, methane chemical vapor infiltration (CVI) processes were studied in the past years for manufacturing components for space application such as using in engines as nozzle throat section for launchers [11, 12].

Concerning the C/C application in spacecraft TPS, it has to be mentioned that in low Earth orbit (LEO) environment, C/C naked materials will suffer oxidation, thus downgrading their performances, when long-standing space missions are planned. At present, many advanced oxidation protection systems have been developed, but there is no universal solution for the general problem of protecting C/C against oxidation [13], in particular for long missions in LEO regions where the issue of high-energy atomic oxygen erosion must be considered [14, 15]. Oxidative phenomena in carbon-based ceramic materials determine multiple issues: layers' delamination occurs when the fiber/matrix interface is engaged, while fiber bundles cracks may arise at growing temperatures. To prevent materials' oxidation, two approaches are typically pursued: suppressing the degradation rate by blocking the inner active sites by using inhibitors and sealants, or hindering oxygen reaction with carbon by means of outer surface coating treatment [16, 17]. At present, a broad variety of procedures are exploited for coating formulation and applying techniques, such as deposition of ceramic layers by batch carburizing, reaction sintering, or matrix impregnation and pyrolysis. In particular, silicon carbide (SiC) ceramic is widely used as a coating to provide protection against oxidation owing to its excellent anti-oxidation properties and good compatibility with C/C composites;

moreover, the glassy SiO_2 film formed on the surface of the coating while the SiC coated C/C composites are subject to oxidative agents at high temperature can efficiently prevent oxygen from diffusing into the C/C matrix [18]. For ceramic coating deposition, using the CVD technique dense coating layers is possible with good adhesion to the substrate; however, due to the low deposition rates, the processing times are high, thus increasing the manufacturing process cost, and, furthermore, there is a strong limitation for the component size due to the high vacuum chamber technology and gas feed stream necessary [19]. Furthermore, disadvantages such as degrading of the substrate material after the coating application or flaking phenomena caused by a weak coating adhesion have not yet been suitably addressed. Thus, the modern aerospace research industry efforts are devoted to develop improved coating products and processes.

This work describes a coating technique consisting in the spreading of a commercial refractory paint reinforced with ceramic nanopowders over C/C substrates: the main aim is to assess a process characterized by time/cost-saving while retaining performances in terms of substrate's surface preservation from thermal oxidation [20, 21]. The proposed coating capability is investigated performing a full thermal properties characterization by means of an advanced numerical approach (known as inverse method [22, 23]) combined with a detailed experimental analysis, allowing to estimate with optimal accuracy the materials' thermal conductivity and heat capacity over a wide range of temperatures. The modern approaches to design the considered materials assume broad application of mathematical and physical simulation methods. Anyway, mathematical simulations are reliable only if approved information is available about the specific properties of the objects under investigation. Generally, the direct measurement of the materials' thermophysical properties, especially in the case of hybrid composition structures, is actually impossible, the only way to overcome such complexities being indirect measurement. From the computational point of view, such an approach is usually formulated as a solution of the inverse problem: through direct measurements of the system's state (temperature, component concentration, etc.), its properties, as the materials' thermophysical characteristics, are defined. Violations of cause-and-effect relations in the statement of these problems results in their correctness in a mathematical sense (i.e., the absence of existence and/or uniqueness and/or stability of the solution). Hence, special methods usually called as 'regularized' have been developed to deal with such problems in the most suitable route.

2 C/C-Coated Materials

C/C composites are a typology of hierarchical ceramic materials constituted by a graphitic bulk coupled to a carbon fiber preform. They have significant thermal stability and resistance, which allow to retain excellent mechanical properties at very high temperatures: such feature, in view of the relative lightness with respect to conventional metallic materials, suggests their employment in particular as component for spacecraft structures and subsystems. Industrial C/C tiles (Mitsubishi Chemical Carbon Fiber and Composites—density around 1.45 g/cm^3) were machined to extract several samples: rectangular panels (sides ~ 12×5 cm^2, thickness 4 mm) for the thermal conductivity and heat capacity testing are shown in Fig. 1. The C/C plates were pre-conditioned in low pressure environment (8 h at ~ 10^{-5} mbar) to remove contaminations and minimize moisture absorption effects. A ceramic pyro-paint (Aremco Products) was adopted as the main coating component: it is a high-melting Al/oxide-based varnish able to operate in very harsh thermal conditions (up to 1800 °C, [20, 21]). The paint was filled by

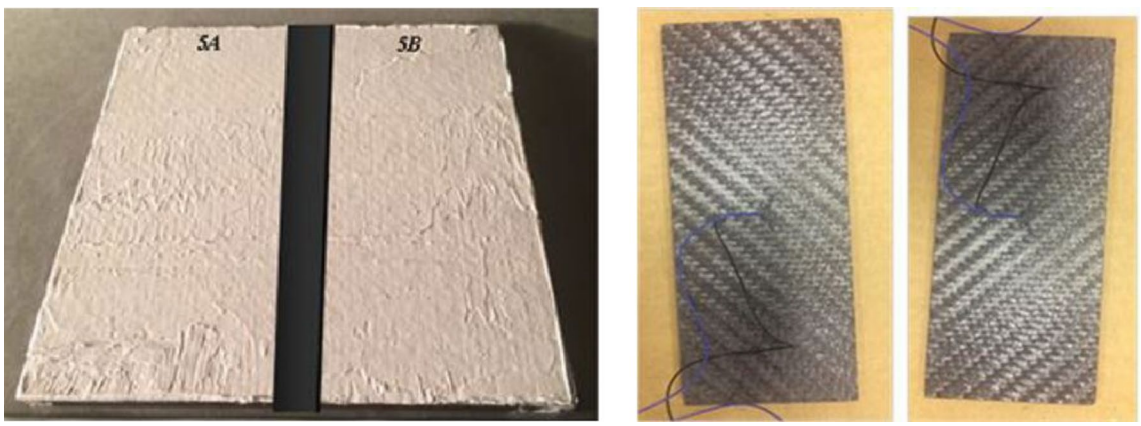

Fig.1 A square tile cut out from commercial C/C slab, split in half for the thermal characterization: coated surface (left), back surface (right)

inclusion of Si/oxide nanopowders (Sigma-Aldrich—nSiO_2: av. diameter 12 nm, surface area 175–225 m^2/g) at different weight percentages (0.0–1.0 wt%): such ceramic materials are typically employed to increase the insulating properties by lowering the thermal conductivity [13, 15, 19]. The as-manufactured mixtures were brushed over the C/C panels, leveling the free surface to achieve a coating thickness in a range 0.3–0.6 mm; after the application, the hybrid samples were cured by following the pyro-paint technical specifications (2 h in air dry, 2 h at 98 °C, and 1 h at 427 °C).

3 Thermal Test

The characterization of coated C/C material was carried out with the aim of evaluating the material thermal properties by inverse problems technique. Five typologies of materials were tested—i.e., C/C with bare coating and enriched with silica nanoparticles at 0.25, 0.50, 0.75 and 1.00 wt%. Two specimens for each material were submitted for thermal tests as a rectangular parallelepiped (see Fig. 1): the adopted experimental sample was a slab taken from the material under investigation with major edge thickness-to-length ratio about 1:25. The labeling, weight and sizes of the ten specimens are indicated in Table 1. The adopted dimensioning, as well as the use of two identical specimens' symmetrical heating procedure, provided a thermal profile close to a one-dimensional framework in the course of testing, with initially uniform temperature distribution along the specimen. A number of thermocouples (wires thickness 0.05 mm) were installed on the heating and back surfaces of the specimens (Fig. 2), since the analyzed material is electrically conductive, as well as on the specimens' heating surfaces into the thin surface dimples with isothermal area 6 mm length, fixed by high-temperature adhesive and output back throughout the specimen slots. The heat flux sensors in the form of rectangular slab made from SiO_2 fibers were positioned on the specimens' back surfaces to provide inverse problems unique solution. The sensor thickness was selected during the process of pilot tests with the help of measured conditions of temperature reaction on the back surface. The experiment facilities TVS-2 M and the experimental module EM-2B, with heating element (HE) made from stainless steel strip 0.1 mm thick, were used for the test execution (Fig. 3). The control system based on PXI tools was used for heating manipulation, measurements and data collecting. The pilot tests have shown that the analyzed material has great electrical conductivity, which arises during the increase of temperature; at temperature greater than 120 °C, it is comparable to the HE material electrical conductivity. This property creates serious problems during the realization of the test scheme, demanding electrical isolation of thermocouples wires from HE material. The symmetric scheme of the heating of two similar specimens (Ai and Bi, $i=1, \ldots, 5$) by steel HE was chosen for test execution. The temperature measurement scheme is presented in Tables 2 and 3. The specimens' heating program was chosen during the pilot tests, based on the assessment of a given maximum temperature of specimen heating $T_{1MAX}(\tau) \sim 400$ °C, thus ensuring an acceptable temperature measurement at specimens' back surfaces as well as not exceeding HE temperature of $T_{HE\text{-}MAX}(\tau) \sim 470$ °C, which is critical for electrical isolation covering of HE and thermocouples. The results of the temperature measurements for Ai specimens are presented in Figs. 4, 5, 6, 7 and 8.

4 Inverse Problems Technique

Based on the given physical model, a mathematical model of heat transfer process in the material's specimen (infinite three-layer slab of known thickness) can be presented as follows:

Table 1 Specimens' parameters

Specimen	Length (mm)	Width (mm)	Thickness[a] (mm)	Density[b] (kg/m^3)	n-SiO_2 (%)
A1	120.1	50.6	4.45	1387	0
B1	120.1	50.4	4.30	1422	0
A2	119.8	48.8	4.53	1385	0.25
B2	120.1	49.2	4.59	1383	0.25
A3	120.0	48.9	4.60	1358	0.5
B3	120.0	49.5	4.53	1348	0.5
A4	120.2	49.0	4.45	1270	0.75
B4	118.4	49.0	4.39	1333	0.75
A5	120.7	50.3	4.55	1376	1.0
B5	120.7	50.1	4.50	1378	1.0

[a]Average value by five measurements

[b]Calculated

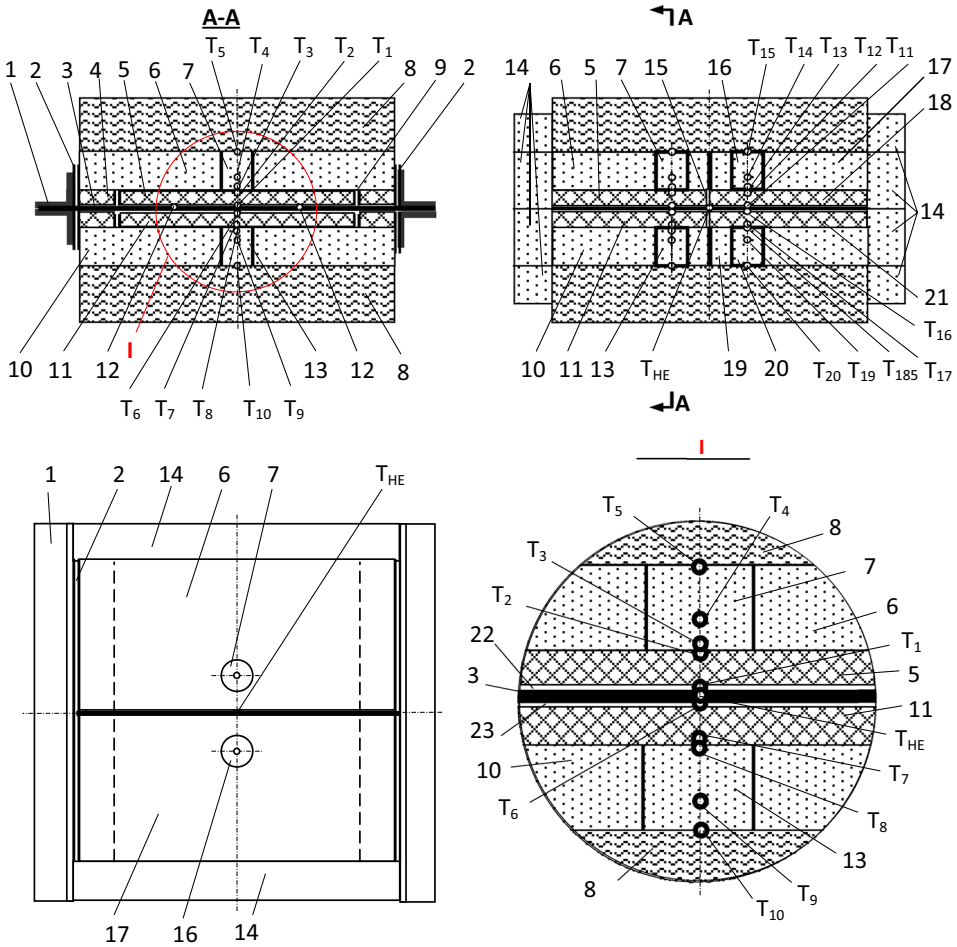

Fig. 2 Testing scheme: 1—holder of the heating element (HE), 2—thermoelectrical insulation, 3—heating element, 4—holder of specimen, 5—experimental specimen A1, 6—heat flux sensor on the specimen A1, 7—measuring element of sensor on A1, 8—thermal isolation, 9—thermoelectrical isolation, 10—heat flux sensor on the specimen B1, 11—experimental specimen B1, 12—points of voltage measurement on HE, 13—measuring element of sensor on B1, 14—clamping plate. 15—thermoelectrical isolation, 16—measuring element of sensor on A2, 17—heat flux sensor on the specimen A2, 18—experimental specimen A2, 19—heat flux sensor on the specimen B2, 20—measuring element of sensor on B2, 21—experimental specimen B2, 22—coating of specimens A, 23—coating of specimens B. Thermocouples: T_{HE}—control thermocouple on HE, T_1—on the heating surface of specimen A1, T_2—on the back surface of specimen A1, T_3—on the heat flux sensor heating surface of specimen A1, T_4—internal in the heat flux sensor heating surface of specimen A1, T_5—on the heat flux sensor back surface of specimen A1, T_6—on the heating surface of specimen B1, T_7—on the back surface of specimen B1, T_8—on the heat flux sensor heating surface of specimen B1, T_9—internal in the heat flux sensor heating surface of specimen B1, T_{10}—on the heat flux sensor back surface of specimen B1, T_{11}—on the heating surface of specimen A2, T_{12}—on the back surface of specimen A2, T_{13}—on the heat flux sensor heating surface of specimen A2, T_{14}—internal in the heat flux sensor heating surface of specimen A2, T_{15}—on the heat flux sensor back surface of specimen A2,, T_{16}—on the heating surface of specimen B2, T_{17}—on the back surface of specimen B2, T_{18}—on the heat flux sensor heating surface of specimen B2, T_{19}—internal in the heat flux sensor heating surface of specimen B2, T_{20}—on the heat flux sensor back surface of specimen B2

$$C_l(T)\frac{\partial T_l}{\partial \tau} = \frac{\partial}{\partial x}\left(\lambda_l(T)\frac{\partial T_l}{\partial x}\right),$$

$$X_{l-1} < x < X_l,\ l = \overline{1,3},\quad 0 \le \tau \le \tau_{\max}, \tag{1}$$

$$T_l(x,0) = T_l^0(x),\ X_{l-1} < x < X_l,\ l = \overline{1,3}, \tag{2}$$

$$-\lambda_1(T)\frac{\partial T_1(X_0,\tau)}{\partial x} = q_1(\tau),\quad \tau \in (\tau_{\min}, \tau_{\max}], \tag{3}$$

$$\lambda_l\left(T_l(X_l,\tau)\right)\frac{\partial T_l(X_l,\tau)}{\partial x} = \lambda_{l+1}\left(T_{l+1}(X_l,\tau)\right)\frac{\partial T_{l+1}(X_l,\tau)}{\partial x}, l = 1,2, \tag{4}$$

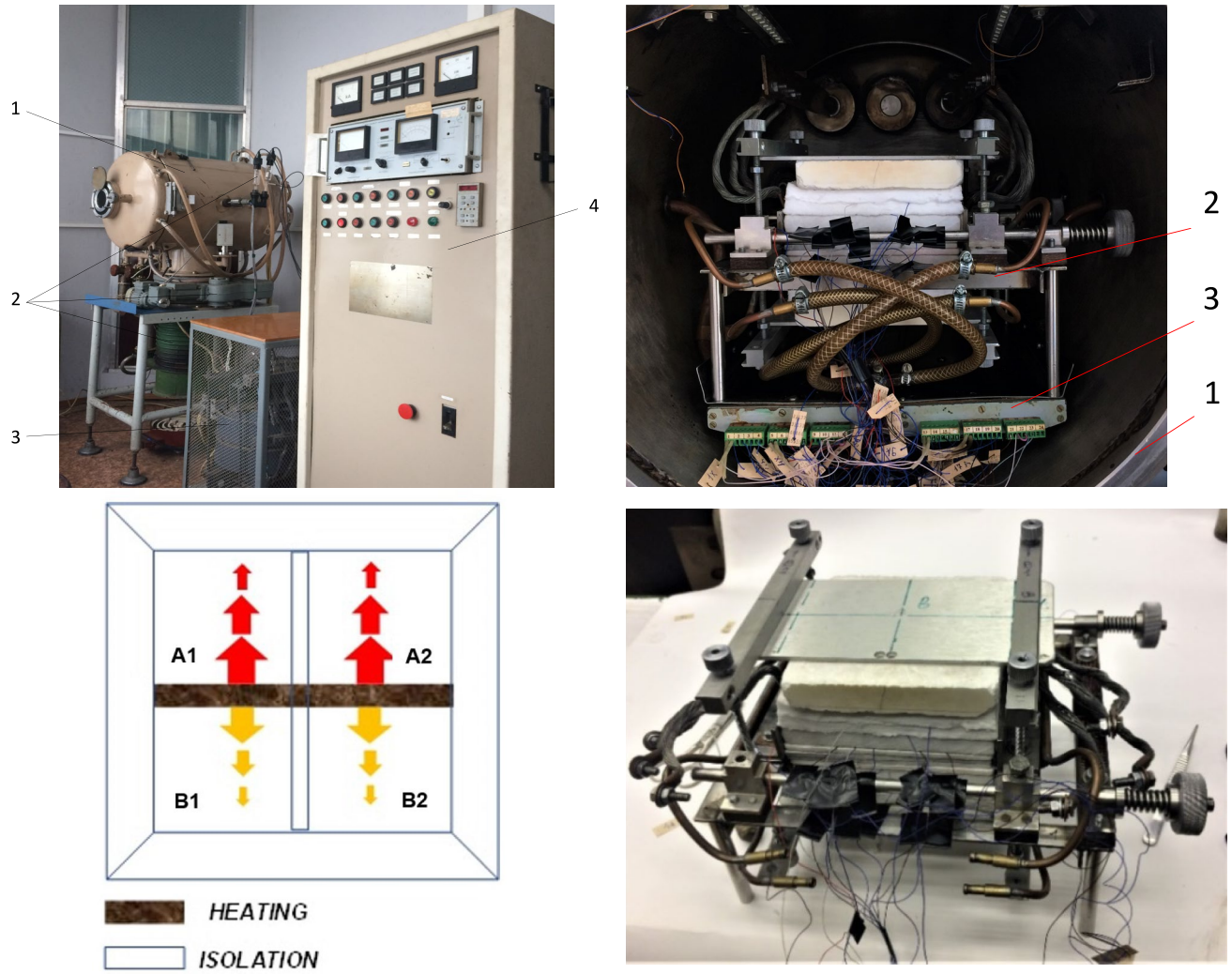

Fig. 3 Experimental setup for heat transport analysis. top—on the left, a general view of TVS-2 M stand: 1—vacuum chamber, 2—vacuum system, 3—power system, 4—monitoring and control rack; on the right, inside of the vacuum chamber of TVS-2M stand: 1—vacuum chamber, 2—experimental module EM-3D, 3—connector blocks of thermocouples. Down—simplified schematics illustrating the heat transport measuring concept (left), the experiment module with installed specimens and thermos-insulating holder (right)

Table 2 Thermal measurement scheme by specimens

Coordinate (mm) Thermo-couple	A1	A2	A3	A4	A5	B1	B2	B3	B4	B5
X_1	0, 0	0, 0	0, 0	0, 0	0, 0	0, 0	0, 0	0, 0	0, 0	0, 0
T_i	T_1	T_{11}	T_{11}	T_{11}	T_{11}	T_6	T_{16}	T_{16}	T_{16}	T_{16}
X_2	4, 45	4, 53	4, 60	4, 45	4, 55	4, 30	4, 59	4, 53	4, 39	4, 50
T_i	T_2	T_{12}	T_{12}	T_{12}	T_{12}	T_7	T_{17}	T_{17}	T_{17}	T_{17}

$$T_l(X_l, \tau) = T_{l+1}(X_l, \tau), \quad l = 1, 2, \tag{5}$$

$$-\lambda_3(T)\frac{\partial T(X_3, \tau)}{\partial x} = q_2(\tau), \quad \tau \in (\tau_{\min}, \tau_{\max}]. \tag{6}$$

In the modeling described by Eqs. (1)–(6), the coefficients $C_1(T)$ and $\lambda_1(T)$ as well as $C_2(T)$ and $\lambda_2(T)$ are

Table 3 Thermal measurement scheme by thermal flux sensors

Coordinate (mm) Thermocouple	Sensor on A1	Sensor on A2…A5	Sensor on B1	Sensor on B2…B5
X_1	0, 0	0, 0	0, 0	0, 0
T_i	T_3	T_{13}	T_8	T_{18}
X_2	5, 8	5, 8	5, 7	5, 7
T_i	T_4	T_{14}	T_9	T_{19}
X_3	22, 5	22, 5	22, 5	22, 5
T_i	T_5	T_{15}	T_{10}	T_{20}

unknown. The experimental equipment and the measured system presented above could be applied for estimating the unknown functions by inverse problems technique, and the results of temperature measurements inside the specimen are assigned as necessary additional information to solve an inverse problem.

$$T^{\exp}(X_m, \tau) = f_m(\tau), \quad m = \overline{0,2}, \quad . \tag{7}$$

It is impossible to estimate simultaneously the set $C_1(T)$, $\lambda_1(T)$, $C_2(T)$ and $\lambda_2(T)$ by internal temperature measurements; to overcome this problem, additional experiments with C/C material without coating were carried out. Therefore, $C_2(T)$ and $\lambda_2(T)$ were estimated in advance, then $C_1(T)$ and $\lambda_1(T)$ were obtained for different coatings.

Two uniform difference grids are introduced in the interval $[T_{\min}, T_{\max}]$ with the number of nodes N_i, $i=1, 2$, namely

$$\omega_i = \left\{ T_k = T_{\min} + (k-1)\Delta T,\ k = \overline{1, N_i} \right\}, i = \overline{1,2}. \tag{8}$$

The unknown functions on grids (6) are approximated by using cubic B-splines as follows:

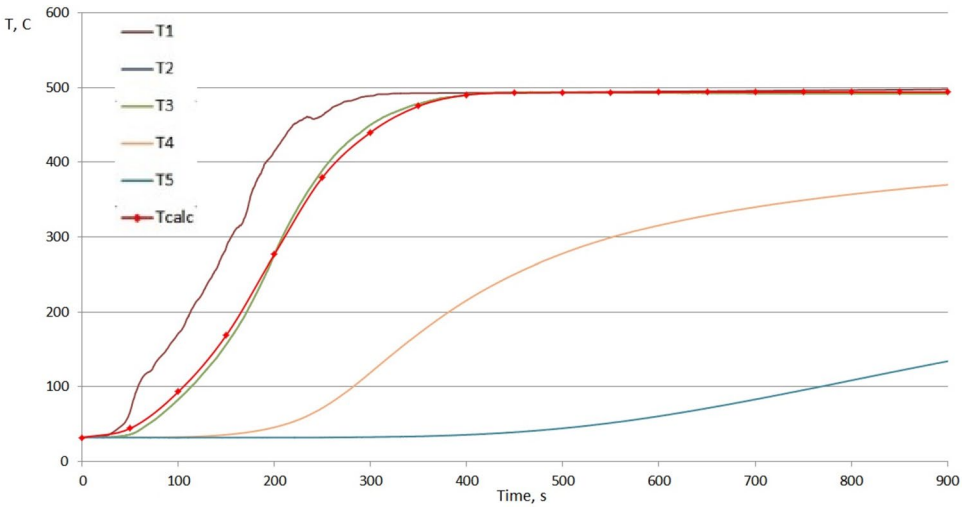

Fig. 4 Measured temperature vs time plotted for specimens A1 (base coating) and comparison with the calculated temperature on the specimen back surface

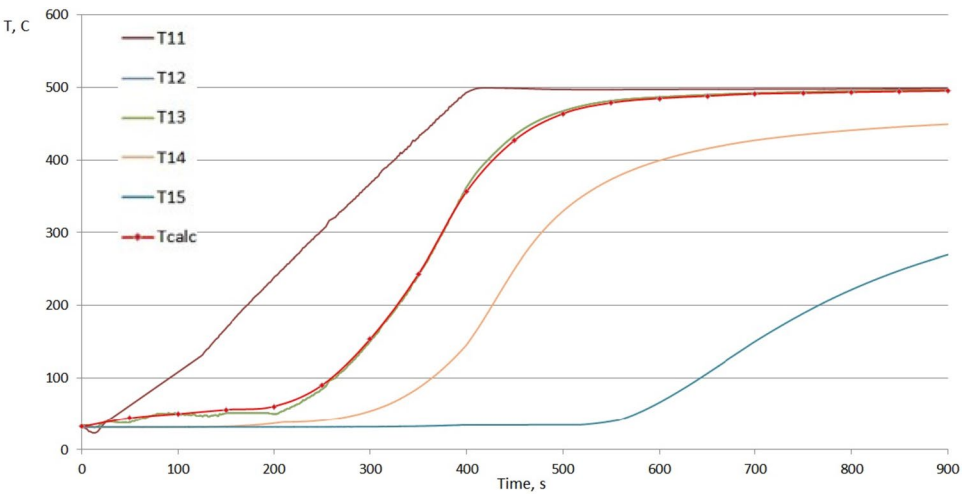

Fig. 5 Measured temperature vs time plotted for specimens A2 (coating reinforced by 0.25% of n-SiO_2) and comparison with the calculated temperature on the specimen back surface

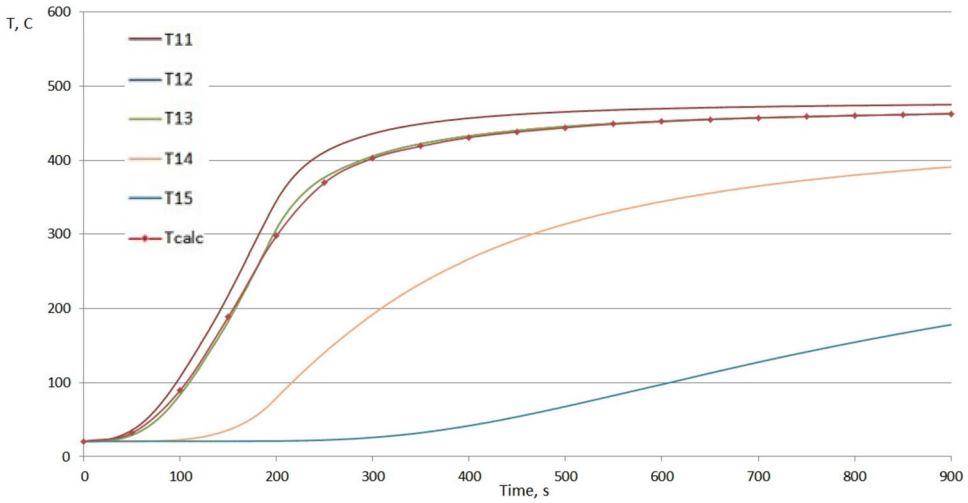

Fig. 6 Measured temperature vs time plotted for specimens A3 (coating reinforced by 0.50% of n-SiO_2) and comparison with the calculated temperature on the specimen back surface

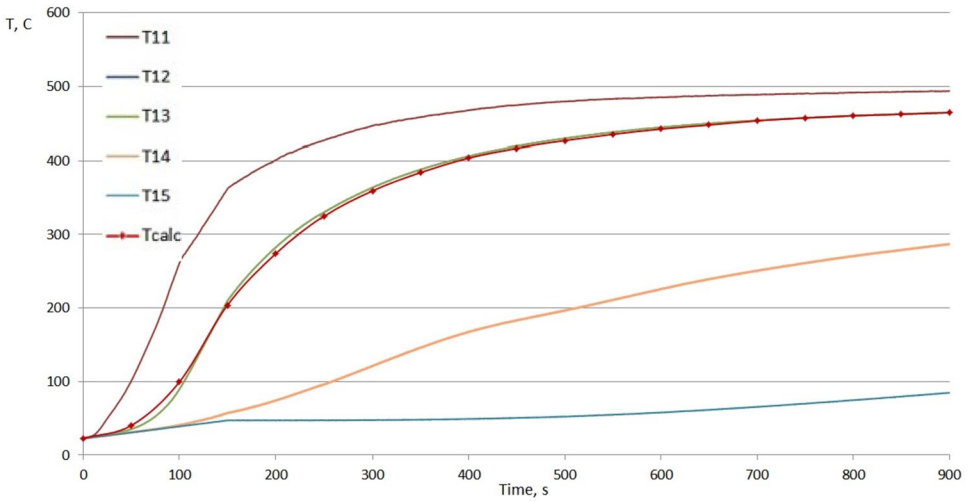

Fig. 7 Measured temperature vs time plotted for specimens A4 (coating reinforced by 0.75% of n-SiO_2) and comparison with the calculated temperature on the specimen back surface

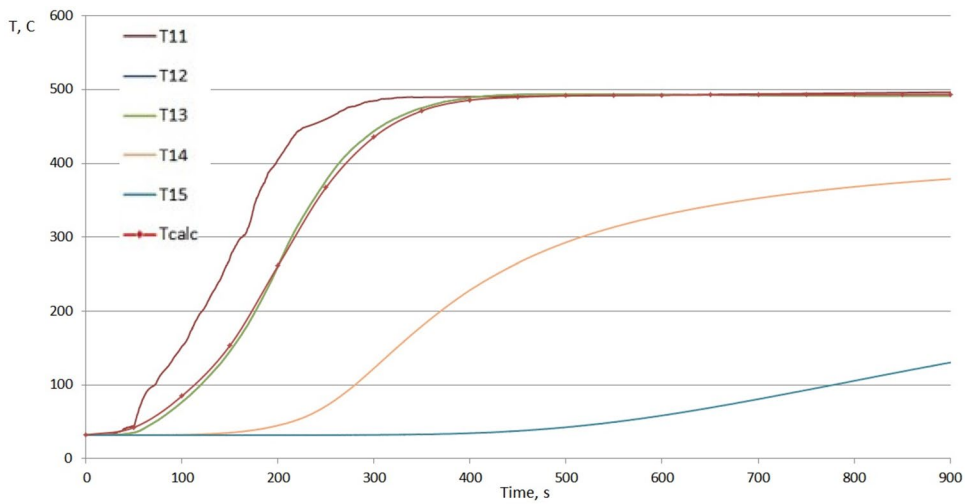

Fig. 8 Measured temperature vs time plotted for specimens A5 (coating reinforced by 1.00% of n-SiO_2) and comparison with the calculated temperature on the specimen back surface

$$C_1(T) = \sum_{k=1}^{N_1} C_k \phi_k^1(T), \qquad \lambda_1(T) = \sum_{k=1}^{N_2} \lambda_k \phi_k^2(T), \tag{9}$$

where C_k, $k=1, N_1$, λ_k, $k=1, N_2$, are parameters. As a result of the approximation, the inverse problem is reduced to search the vector of unknown parameters $\overline{p} = \{p_k\}$, $k=1, N_p$, which has dimension $N_p = N_1 + N_2$. The least-square residual of computational and measured temperatures at the points of the thermocouple installation is given by

$$J\big(C_1(T),\ \lambda_1(T)\big) = \sum_{m=0}^{1} \int_{\tau_{\min}}^{\tau_{\max}} \big(T\big(X_m,\ \tau\big) - f_m(\tau)\big)^2 d\tau, \tag{10}$$

where $T(X_{\mathrm{m}}, \tau)$ is defined from a solution of the boundary-value problem (1)–(6).

It is assumed here that the conditions of uniqueness of the inverse problem solving are satisfied. An iterative regularization method stated here, according to the general definition of Tikhonov's regularizing operators, gives rise to a regularizing set of operators, in which a regularization parameter is the number of the last iteration. For linear ill-posed problem, the iterative regularization method has received a rigorous mathematical proof and practical verification through data of mathematical modeling. Applicable to nonlinear problems, there are at present no complete theoretical results on the substation of iterative algorithm stability. However, the results of computational experiments already made in solving the inverse heat transfer problems of different types prove the high efficiency of the iterative regularization method as well as the possibility to analyze a wide range of nonlinear problems.

Proceeding from the principle of iterative regularization, the unknown vector can be determined through the minimization of the functional (10) by gradient methods of the first-order prior to the fulfillment of the condition:

$$J(\overline{p}) \le \delta_f,\ \delta_f = \sum_{m=0}^{2} \int_{\tau_{\min}}^{\tau_{\max}} \sigma_m(\tau)\, \mathrm{d}\tau, \tag{11}$$

where the integral error of the temperature measurements $f_m(\tau)$ is defined, σ_{m} being the measurement variance.

To construct the iterative algorithm for this inverse problem, the solution of a conjugate gradient method is used. A successive approximation process is constructed as follows:

(i) a priori an initial approximation of the unknown parameter vector $\overline{p}^0$ is set;

(ii) a value of the unknown vector at the next iteration is calculated as follows:

$$\overline{p}^{s+1} = \overline{p}^s + \gamma^s \overline{g}^s$$
$$\overline{g}^s = -\overline{J'}^s + \beta^s \overline{g}^{s-1},$$

$$\beta^0 = 0, \beta^{\mathrm{s}} = \left\langle \left(\overline{J_p'^{(s)}}, \left(\overline{J_p'^{(s-1)}}\right)\right), J_p'^{(s)} \right\rangle \tag{12}$$

where $\overline{J'}_p^{(s)}$ is the value of the functional gradient at the current iteration. The greatest difficulties in realizing the gradient methods are connected with the calculation of the minimized functional gradient. In the developed approach, the methods of calculus of variations is used. Here, an analytic expression for the minimized functional gradient is obtained:

$$\frac{\partial J}{\partial \mathrm{O}} \tag{13}$$

$$\frac{\partial J}{\partial C_k} \equiv J_{C_k}{}'$$
$$= -\sum_{l=1}^{3} \int_0^{\tau_{\max}} \int_{X_{l-1}}^{X_l} \psi_l(x,\tau) \frac{\partial T_3}{\partial \tau} \phi_k(T) \mathrm{d}x \mathrm{d}\tau, \tag{14}$$
$$k = \overline{1, N_C},$$

where $\psi(x, \tau)$ is the solution of a boundary-value problem adjoint to a linearized form of the direct problem (1)–(6):

$$C_l(T) \frac{\partial \psi_l}{\partial \tau} = \frac{\partial}{\partial x}\left(\lambda_l(T) \frac{\partial \psi_l}{\partial x}\right) - \left(\frac{d\lambda_l}{dT} \frac{\partial T_l}{\partial x}\right) \frac{\partial \psi_l}{\partial x}, \tag{15}$$

$$X_{l-1} < x < X_l,\ l = \overline{1,3},$$
$$0 \le \tau \le \tau_{\max},$$

$$\psi_l\big(x, \tau_{\max}\big) = 0, X_{l-1} \le x \le X_l,\ l = \overline{1,3}, \tag{16}$$

$$\lambda_1\big(T_1\big(X_0, \tau\big)\big) \frac{\partial \psi_1\big(X_0, \tau\big)}{\partial x} = 2\big[T_1\big(X_0, \tau\big) - f_l(\tau)\big], \tag{17}$$

$$\lambda_1\big(T_1\big(X_1, \tau\big)\big) \frac{\partial \psi_1\big(X_1, \tau\big)}{\partial x} = \lambda_2\big(T_2\big(X_1, \tau\big)\big) \frac{\partial \psi_2\big(X_1, \tau\big)}{\partial x}, \tag{18}$$

$$\psi_{l-1}\big(X_l, \tau\big) = \psi_l\big(X_l, \tau\big),\quad l = 1, 2, \tag{19}$$

$$\lambda_2\big(T_2\big(X_2, \tau\big)\big) \frac{\partial \psi_2\big(X_2, \tau\big)}{\partial x} - \lambda_3\big(T_3\big(X_3, \tau\big)\big) \frac{\partial \psi_3\big(X_2, \tau\big)}{\partial x} = 2\big[T_2\big(X_2, \tau\big) - f_2(\tau)\big], \tag{20}$$

$$\lambda_3\big(T_3\big(X_3, \tau\big)\big) \frac{\partial \psi_3\big(X_3, \tau\big)}{\partial x} = 0. \tag{21}$$

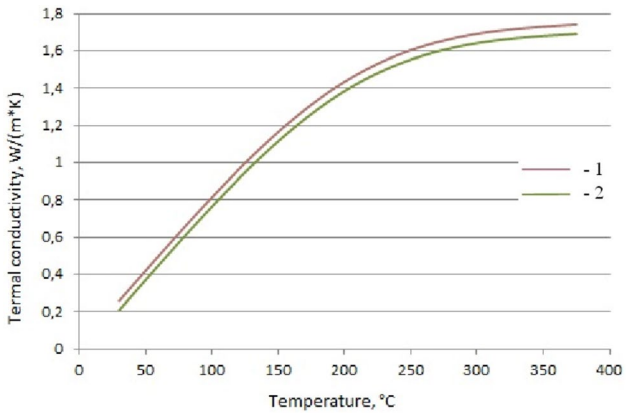

Fig. 9 Estimated thermal conductivity as function of temperature of naked C/C plates: 1—A0, 2—B0

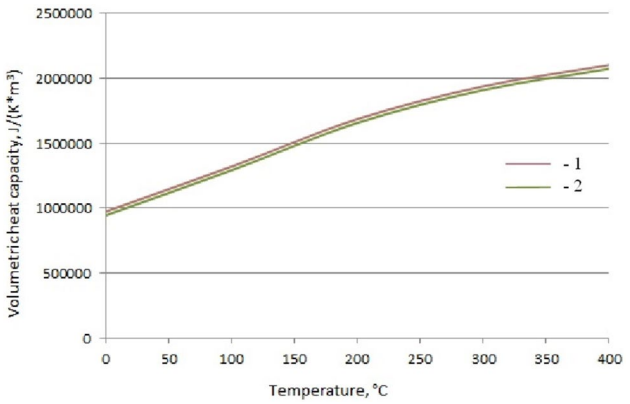

Fig. 10 Estimated heat capacity as function of temperature of naked C/C plates: 1—A0, 2—B0

The estimation of the functions $C(T)$ and $\lambda(T)$ for previously analyzed C/C naked substrate (two similar samples labeled as A0 and B0) and in the present case of different coatings is reported in Figs. 9, 10 and 11, 12, respectively. Table 4 includes the obtained values of the least squares methods and the maximum deviation of the temperatures calculated from those measured during the experiments.

5 Result Analysis

All the tested samples showed very good thermal stability over a wide range of temperatures. Remarkable coincidences have been assessed by comparing the temperature/time recorded by the "matched" thermocouples (i.e., the temperature trend in the corresponding regions of two similar specimens, Ai and Bi, was found to be fully congruent within the limits of the experimental uncertainties), thus ensuring a high level of confidence provided by the test equipment in terms of results reproducibility. Moreover, the comparison between measured and calculated temperature on the specimens back side (see Figs. 4, 5, 6, 7 and 8, where T_2/T_3 and T_{12}/T_{13} are almost undistinguishable due to their closer housing, as depicted in the testing scheme reported in Fig. 2) presents good accordance, thus establishing the robustness of the proposed approach. A decrease in temperature between the front and back sides was found in the range 50–100 °C, which corresponds to a thermal "delay" of about 15 s, almost constant throughout the entire time interval under the selected heating conditions.

The estimation of the thermal conductivity $\lambda(T)$ and heat capacity $C(T)$ functions by solving the inverse method (see

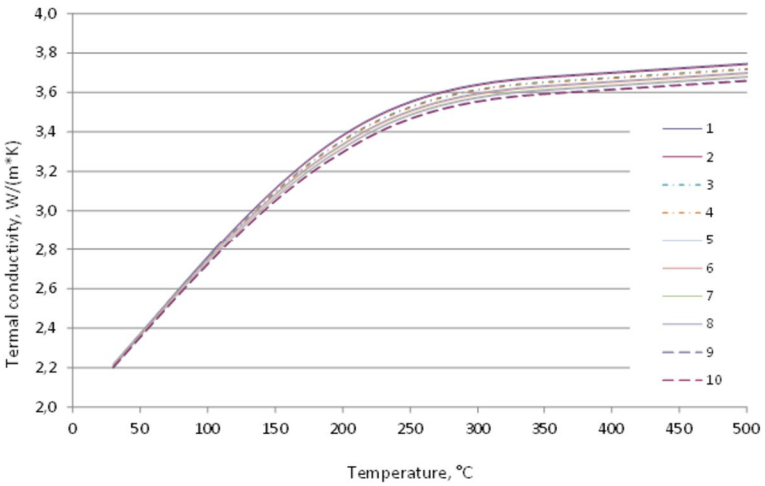

Fig.11 Estimated thermal conductivity as function of temperature of coated materials: 1, 2—specimens A1, B1 (0% n-SiO_2), 3, 4—specimens A2, B2 (0.25% n-SiO_2), 5, 6—specimens A3, B3 (0.5% n-SiO_2), 7, 8—specimens A4, B4 (0.75% n-SiO_2), 9, 10—specimens A5, B5 (1.0% n-SiO_2)

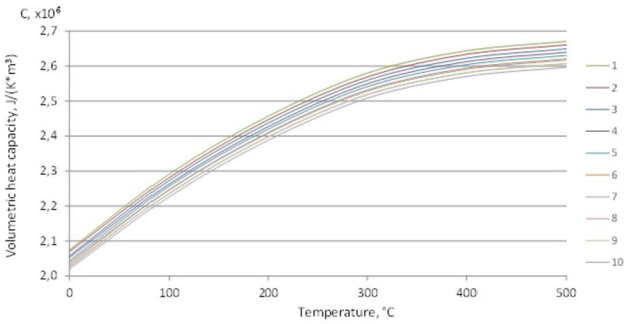

Fig. 12 Estimated heat capacity as function of temperature of coated materials: 1, 2—specimens A1, B1 (0% n-SiO_2), 3, 4—specimens A2, B2 (0.25% n-SiO_2), 5, 6—specimens A3, B3 (0.5% n-SiO_2), 7, 8—specimens A4, B4 (0.75% n-SiO_2), 9, 10—specimens A5, B5 (1.0% n-SiO_2)

Table 4 Difference between estimated and measured temperatures

Specimen	Least-squares temperature deviation (K)	Maximum temperature deviation (K)
A1	1.32	5.3
B1	1.24	4.9
A2	1.21	5.0
B2	1.26	4.6
A3	1.23	4.5
B3	1.29	4.9
A4	1.30	5.1
B4	1.19	4.7
A5	1.28	4.4
B5	1.22	4.5

Figs. 9, 10, 11 and 12) firstly shows how the presence of the coating highly affects the thermophysical properties of the C/C substrate. In particular, both thermal conductivity and volumetric heat capacity are systematically raised in the coated material all over the temperature range considered, with asymptotic values almost threefold for what concerns the conductivity (around 3.7 W/m·K vs. 1.7 W/m·K for the naked C/C up to 400 °C) and increased by about 25% for the capacity (2.65×10^6 J/m^3·K on average vs. 2.10×10^6 J/m^3·K for the naked C/C up to 400 °C). Such behavior is surely appropriate if a substrate with high thermal stability as C/C has to be protected from an oxidizing environment, by preserving at the same time the whole structural integrity against huge thermal stress. Considered as bulk material, in fact, the surface layer conducts heat to the inner part without excessive increase of its own temperature, thus reducing simultaneously the detrimental effect of surface oxidation and the occurrence of thermal-induced cracks or delamination.

As far as the influence of silica nanopowder addition to the base varnish coating is concerned, the results outlined in Figs. 11, 12 for the estimated thermal conductivity and volumetric heat capacity of the several coated materials as function of temperature suggest that there is a no significant disorder effect on the Al/oxide-based matrix, even if the gradual inclusion of insulating nanoparticles leads to a little decrease of both thermal conductivity and heat capacity, by about 2.5% and 2.8% when temperature rises toward the maximum of 500 °C, respectively. This feature implies the reliability of the hybrid-multiscale coating approach, since TPS shielding is not achieved by adding layers—i.e., changing materials and construction, and thus making the entire structure heavier—but only improving the intrinsic physical properties of the base matrix.

The latter results can be directly correlated to that previously observed from the CTE characterization of this kind of materials [21, 24], since a little higher expansion can be considered as responsible for a slight lowering of heat conduction/exchange in ceramic materials. Moreover, it is worth noting that such structural upgrade does not give rise to overheating drawbacks, since the material volumetric heat capacity sounds as almost unaffected by the nanoinclusions. Definitely, considering the combined CTE-$\lambda(T)$ behavior, it can be assessed that the proposed multiscale ceramic hierarchical architecture may lead to the formation of a more resilient coating, thus optimizing the main functionality of C/C protection from erosion and oxidation. Previously performed elemental analysis of the coating layer evaluated the composition of the alumina and silica in the coating solution, confirming the very low carbon species content. Further efforts are surely needed to optimize the substrate/coating interface physical properties, to achieve a suitable degree of adhesion by maximizing the coating embedding within the C/C bulk. Basically, the reported results indicate the proposed hybrid ceramic coating as a feasible technical strategy to preserve TPS C/C substrate from the space environment oxidative conditions, thanks to both an improved protection effectiveness and LCC safety.

6 Conclusions

In this work, an experimental thermal analysis of a novel coating material for protecting a carbon–carbon composite surface was carried out. A commercial product made of an alumina-based refractory varnish was enriched with the inclusion of silica nanoparticles aimed at increasing the oxidation resistance without losing thermomechanical stability, adhesion and uniformity. The complete thermal characterization was carried out by experimental and numerical analysis of the coated materials with various concentrations of n-SiO_2 addition (0.0–1.0 wt%). In particular, the advanced

inverse method was adopted for assessing the thermophysical properties such as heat capacity and thermal conductivity of the manufactured materials in a broad range of temperatures, by exploiting the input of an in-house developed experimental setup. The main results of the present study were:

- establishing the reliability of the materials' manufacturing methodology and of the experimental framework designed, as well as the robustness of the mathematical approach adopted, as testified by the results reproducibility revealed during similar samples testing and by the agreement between measured and calculated values of temperatures throughout the whole thermal range explored;
- confirming the effectiveness of the hybrid ceramic coating strategy proposed, since the experimental and numerical results of the thermophysical characterization of the manufactured specimens outlined that the applied surface layer would be able to prevent C/C substrate oxidation without degradation due to high thermal loading;
- promoting the use of ceramic nanosized addition to commercial refractory varnish to improve the overall protective coating performances, since the improved resistance to oxidation given by silica-based material does not lead to a significant weakening of the structure in terms of thermal stability; in this regard, the experimental and numerical analysis of thermal conductivity and heat capacity revealed a slight decrease in the heat transfer characteristics of the nanostructured coating, confirming previously reported results about the thermomechanical analysis of the proposed materials.

The presented results point out that the proposed hybrid ceramic coating represents a possible technical strategy for protecting TPS from the detrimental space environment conditions, with specific regard to the huge thermal shock (aerothermal heating up to 10^4 W/cm^2 for entry velocities around 11 km/s, temperatures up to 2000 K for about ten minutes) experienced on the spacecraft exposed surfaces during re-entry phase.

Acknowledgements The contribution of MAI's team was supported by the Russian Science Foundation (Grant no. 18-19-00492).

Funding Open access funding provided by Università degli Studi di Roma La Sapienza within the CRUI-CARE Agreement.

Data availability The datasets generated during and/or analysed during the current study are available from the corresponding author on reasonable request.

Declarations

Conflict of interest On behalf of all authors, the corresponding author states that there is no conflict of interest.

References

1. Finckenor, M.M., de Groh, K.K.: Space Environmental Effects—A Researcher's Guide to: International Space Station, NASA ISS Program Science Office, 2015.
2. Yang, J.C., de Groh, K.K.: Materials issues in the space environment. MRS Bull. **35**, 12–19 (2010)
3. James, B.F., Norton, O.W., Alexander, M.B.: The natural space environment: effects on spacecraft, NASA STI/Recon Technical Report N 95, 25875 (1994)
4. Dever, J.A., Banks, B.A., de Groh, K.K., Miller, S.K.: Degradation of spacecraft materials. In: Kutz, M. (ed.) Handbook of Environmental Degradation of Materials, pp. 465–501. William Andrew Publ, Norwich (2005)
5. Grossman, E., Gouzman, I.: Space environment effects on polymers in low earth orbit. Nucl. Instrum. Methods Phys. Res. B Beam Interact. Mater. Atoms **208**, 48–57 (2003)
6. Pastore, R., Delfini, A., Albano, M., Vricella, A., Marchetti, M., Santoni, F., Piergentili, F.: Outgassing effect in polymeric composites exposed to space environment thermal-vacuum conditions. Acta Astr. **170**, 466–471 (2020)
7. Windhorst, T., Blount, G.: Carbon-carbon composites: a summary of recent developments and applications. Mater. Des. **18–1**, 11–15 (1997)
8. Morgan, P.: Carbon Fibers and Their Composites. Taylor & Francis Group, Sarasota (2005)
9. Sheehan, J.E., Buesking, K.W., Sullivan, B.J.: Carbon–carbon composite. Annu. Rev. Mater. Sci. **24**, 19–44 (1994)
10. Savage, G.: Carbon–Carbon Composites, pp. 277–322. Chapman & Hall, London (1993)
11. Albano, M., Delfini, A., Pastore, R., Micheli, D., Marchetti, M.: A new technology for production of high thickness carbon/carbon composites for launchers application. Acta Astronaut. **128**, 277–285 (2016)
12. Albano, M., Pastore, R., Delfini, A., Micheli, D., Volpini, F., Marchetti, M.: Densification of high thickness C/C composites by chemical vapor infiltration. Procedia Eng. **109**, 381–389 (2015)
13. Bacos, M.P.: Carbon–carbon composites: oxidation behavior and coatings protection. J. Phys. **IV**, 51–59 (2010)
14. Liu, X., Cheng, L., Zhang, L., Luan, X., Mei, H.: Behavior of pure and modified carbon/ carbon composites in atomic oxygen environment. Int. J. Miner. Metall. Mater. **21–2**, 190–195 (2014)

15. Dworak, D.P., Soucek, M.D.: Protective space coatings: a ceramer approach for nanoscale materials. Prog. Org. Coat. **47**, 448–457 (2003)
16. Chen, Z., Wu, W., Cheng, H., Liu, Y., Wang, S., Xue, R.: Microstructure and evolution of iridium coating on the C/C composites ablated by oxyacetylene torch. Acta Astronaut. **66**, 682–687 (2010)
17. Shi, X., Jin, X., Yan, N., Yang, L.: Influence of micro-oxidation on joints of C/C composites and GH3044 for large-size aerospace parts. Acta Astronaut. **140**, 478–484 (2017)
18. Fu, Q.-G., Li, H.-J., Shi, X.-H., Li, K.-Z., Sun, G.-D.: Silicon carbide coating to protect carbon/carbon composites against oxidation. Scr. Mater. **52**, 923–927 (2005)
19. Friedrich, C., Gadow, R., Speicher, M.: Protective multilayer coatings for carbon–carbon composites. Surf. Coat. Technol. **151–152**, 405–411 (2002)
20. Delfini, A., Santoni, F., Bisegna, F., Piergentili, F., Pastore, R., Vricella, A., Albano, M., Familiari, G., Battaglione, E., Matassa, R., Marchetti, M.: Evaluation of atomic oxygen effects on nanocoated carbon-carbon structures for re-entry applications. Acta Astronaut. **161**, 276–282 (2019)
21. Delfini, A., Pastore, R., Santoni, F., Piergentili, F., Albano, M., Alifanov, O., Budnik, S., Morzhukhina, A.V., Nenarokomov, A.V., Titov, D.M., Marchetti, M.: Thermal analysis of advanced plate structures based on ceramic coating on carbon/carbon substrates for aerospace re-entry re-useable systems. Acta Astr. **183**, 153–161 (2021)
22. Alifanov, O.M., Budnik, S.A., Nenarokomov, A.V., et al.: Identification of thermal properties of materials with applications for spacecraft structures. Inverse Probl. Sci. Eng. **12**, 579–594 (2004)
23. Artyukhin, E.A., Ivanov, G.A., Nenarokomov, A.V.: Determination of a complex of materials thermophysical properties through data of nonstationary temperature measurements. High Temp. **31**, 235–241 (1993)
24. Pastore, R., Delfini, A., Santoni, F., Marchetti, M., Albano, M., Piergentili, F., Matassa, R.: Space environment exposure effects on ceramic coating for thermal protection systems. J. Spacecraft Rockets **58**, 1387–1393 (2021)